Post-print version:

POWER TRANSITION CYCLES OF REVERSIBLE SOLID OXIDE CELLS AND ITS IMPACTS ON MICROGRIDS

H. del Pozo Gonzalez, L. Bernadet, M. Torrell, F.D. Bianchi, A. Tarancón, O. Gomis-Bellmunt, J.L. Dominguez-Garcia

BibTex:

```
@Article{del-Pozo-Gonzalez2023,
    Title   = {Power Transition Cycles of Reversible Solid Oxide Cells and its
        Impacts on Microgrids},
    Author  = {Hector del Pozo Gonzalez, Lucile Bernadet, Marc Torrell, Fernando D.
        Bianchi, Albert Tarancón, Oriol Gomis-Bellmunt, Jose Luis Dominguez-Garcia},
    Journal = {Applied Energy},
    Year    = {2023},
    Number  = {},
    Pages   = {121887},
    Volume  = {352},
    Doi     = {10.1016/j.apenergy.2023.121887}
}
```

Power Transition Cycles of Reversible Solid Oxide Cells and its Impacts on Microgrids

Hector del Pozo Gonzalez[a,*], Lucile Bernadet[a], Marc Torrell[a], Fernando D. Bianchi[b], Albert Tarancón[a,d], Oriol Gomis-Bellmunt[c,d] and Jose Luis Dominguez-Garcia[a]

[a]*Catalonia Institute for Energy Research (IREC), Jardins de les Dones de Negre 1, 2ª. - 08930 Sant Adrià de Besòs, Barcelona, Spain*

[b]*Instituto Tecnológico Buenos Aires (ITBA) and Consejo Nacional de Investigaciones Científicas y Técnicas (CONICET), Iguazú 341, C1437, Ciudad Autónoma de Buenos Aires, Argentina.*

[c]*Centre d'Innovacio Tecnologica en Convertidors Estatics i Accionaments (CITCEA), Departament d'Enginyeria Electrica, Universitat Politecnica de Catalunya (UPC), Barcelona 08028, Spain*

[d]*Institució Catalana de Recerca i Estudis Avançats (ICREA), Passeig Lluís Companys 23, 08010 Barcelona, Spain*

ARTICLE INFO

ABSTRACT

Currently, reversible solid oxide cells (rSOC) are the only devices that allows a bidirectional conversion of H_2O and H_2, being able to operate as fuel cell and as electrolyzer. Thanks to the high-temperature operation, rSOC present a higher efficiency and additionally, provide a feasible solution for long-term energy storage in electrical systems. Experimental testing of rSOC have been mainly focused on cells characterization, thermal or degradation analysis, but the study of transition cycles has not been widely studied. The transitions between the operation as a solid oxide fuel cell (SOFC) and as a solid oxide electrolysis cell (SOEC) might have a significant impact on the rest of the electrical system in which the rSOC is integrated. This article analyzes experimentally the power responses of a rSOC stack, during each operating mode (SOEC-SOFC) and during transition between both modes. The results suggest that transition cycles can be achieved in less than 8 minutes and the total transition from SOEC rated power to SOFC rated power in less than 10 minutes, having a significant impact on microgrid operations, especially in islanded mode. The obtained results indicate that the most suitable role for rSOC in a microgrid is as grid-following. The grid-forming role is only possible if the rSOC operates along with a fast-response power source.

1. Introduction

Electrical microgrids have emerged as an effective way to transform traditional networks. The concept divides large systems into multiple small-scale ones with the ability to operate connected to the conventional distribution and isolated grids [1, 2]. In these systems, the role of electrical energy storage is fundamental to mitigate the renewable energy variability and thus make the operation of the entire microgrid more reliable. Reversible solid oxide cells (rSOC), due to their ability to operate as fuel cell and as electrolyzer are an interesting option to perform this role due to their high efficiency. In addition to high efficiency, these devices have fuel flexibility, since the cells have the ability to operate with several type of fuels (e.g. H_2, CO, etc.), which allows their use in combined heat and power (CHP) plants. The global and CHP efficiency of Solid Oxide technology are higher than other technologies such as Proton-Exchange Membrane (PEM) commonly used in applications like transportation or backup power due to its fast start-up time, or alkaline technologies used in the military or aerospace sectors among others [3]. In addition, since rSOC can be used in larger exploitation systems, they result in a more cost-effective

technology as long-term storage in electrical microgrids. A brief comparative of the main technologies is presented in Table 1.

In the literature, it can be found several experimental rSOC studies focused on: degradation analysis [6], materials analysis [7], temperature effects [8] or pressure effects in stacks [9]. However, more in-depth experimental studies are needed to analyze the response times of this type of systems, especially during the transition between the two operation modes: solid oxide fuel cell (SOFC) and solid oxide electrolysis cell (SOEC). Among those, Aicart et al. [10] used a 25 cell stack with 1 kW-4 kW (SOFC-SOEC) rated power to investigate the transitions between electrolyzer mode and fuel cell mode with different fuel composition (H_2 and CH_4). The analysis covers three power levels: minimum, medium power and proposed maximum power, seeking to achieve fast transitions between operating modes without damaging or impairing the performance of the system. The results obtained by the authors suggested that all transition cycles could be performed in an interval of 3 to 10 minutes without negatively affecting stack performance and lifetime. Srikanth et al. [11] presented a comprehensive investigation of a rSOC reactor behavior during mode switching and explored effective transition strategies. They employed a one-dimensional transient reversible solid oxide cell model validated through experiments using a commercially available reactor. One of their main findings revealed that implementing abrupt step changes from SOFC to SOEC or vice versa within a system context is not viable due to the

Table 1
Characteristics of different hydrogen cells for microgrid applications [3, 4, 5]

Technology	Temperature	Fuel Cell Efficiency*	Electrolyzer Efficiency*	Maximum Power**	Warm Start -up time	Role
Proton-exchange membrane	$< 120°C$	$< 60\%$	$< 70\%$	2.5 MW	Short: <1min	Backup
Alkaline	$< 100°C$	$< 50\%$	$< 70\%$	10 MW	Short: <5min	Backup
Solid Oxide	$< 1000°C$	$< 60\%$	$< 85\%$	0.225 MW	Long: >10min	Long-Term

* Nominal system efficiency (LHV) including auxiliaries and heat supply
** Industrial-scale stack maximum power capacity up to 2022: HyLYZER, Aqualizer and Sunfire, respectively.

behavior of BoP components. Finally, a part of a long-term study of a 5/15kW-Class rSOC system, Peters et al. [12] investigated the rSOC dynamics when transitioning from fuel cell to electrolysis mode. Their findings revealed that, in most cases, the switching between these operating modes could be completed in less than three minutes. However, they also stated that when shifting from the fuel cell to the electrolysis mode, a waiting period of approximately 10 minutes was necessary to ensure stable evaporation in the steam generator.

Microgrids including hydrogen energy systems have been analyzed by several authors. Garcia-Torres et al. [13] propose predictive control aimed to achieve an optimal load sharing in a microgrid composed of different types of batteries and two separate PEM-type fuel cell and electrolyzer systems. Quan et al. [14] analyze by simulation a grid-forming control strategy in a microgrid with a PEM-type fuel cell and an electrolyzer. In [15], the authors study a solid oxide fuel cell power plant connected to an AC grid, in which the inverter controls regulate the stack current aiming to ensure a constant power factor of the plant at all possible power levels. Hutty et al. [3] present an economic and suitability study of a microgrid with solar energy, rSOC and battery storage for a residential microgrid, comparing the benefits of the technology against the estimated CAPEX for the microgrid. In [16, 17, 18], the authors analyze the feasibility of systems based on rSOC aimed to supply the electrical and thermal demands of a 20-unit residential flat building and electric and fuel cell vehicles. Motylinski et al [19] study the dynamic response of rSOC in lattice stability applications. The study seeks to identify the capability of these systems to stabilize an electrical network, and their behavior during the switching between SOFC and SOEC modes. The results were experimentally validated with approximated wind profiles. Baldinelli et al. [20] analyze the feasibility of using flywheels to complement the operation rSOC in grid-connected mode, but the rSOC are not modeled in detail.

This article presents an experimental power analysis of rSOC focused on the dynamic behavior during the operation in SOFC and SOEC modes, and also transition cycles between these two modes. The obtained experimental results allow us to evaluate the operation of the rSOC in a microgrid and analyze their possible impact. The article also proposed a control strategy for the proper functioning of the microgrid

with the rSOC inverter operating in grid-following and in grid-forming modes. A detailed description of the system layout, the modelling, and the experimental validation can be found in [21].

The article is structured as follows. Section 2 presents a brief description of rSOC operation and their experimental power responses with different flows, with direct mode changes and respecting the transition cycles to achieve the desired fuel inlet composition. Section 3 focuses on the integration of rSOC in a microgrid introducing the necessary controllers for the proper functioning of the network and the experimental evaluation under several scenarios according to the possible operating modes of the rSOC. Finally, in Section 4 some conclusions are drawn.

2. Experimental Evaluation of Reversible Solid Oxide Cells

2.1. Experimental Set-up

This section presents the working principles of rSOC and their experimental power response under several operating conditions. Figure 1 shows the rSOC setup used in the experimental tests, which is a in-house reversible prototype. The figure also shows the balance of plant (BoP) elements, important for the efficient operation of the entire system. Its hot zone is composed by a furnace where the stack is placed and by two heat exchangers to pre-heat the inlet gases with the outlet ones. The cold zone gathers a steam generator, a condenser to separate the hydrogen and steam from the fuel outlet stream, the gas controllers and power electronics. The studied stack is a commercial stack from SOFCMAN company (China) made up of 30 anode-supported cells with an active surface area equal to 63 cm^2. Its rated power is in the range of $0.7 - 1$ kW (SOFC-SOEC). The parameter values and description of this rSOC can be found in Table 2.

Before increasing the oven temperature and operating the stack, a weight of 120 kg is applied on top to maintain all the layers (cells, interconnects and meshes) sealed all together. Then the furnace temperature is increased by 1 ºC/min to avoid any thermal chock. Once the operating temperature is reached (750 ºC), H_2 is progressively introduced to reduce the fuel electrode. At the end of the reduction process, the stack is ready for operation. SOFC characterization is performed with pure H_2 at the fuel electrode and air at the oxygen electrode, while SOEC characterization needs a
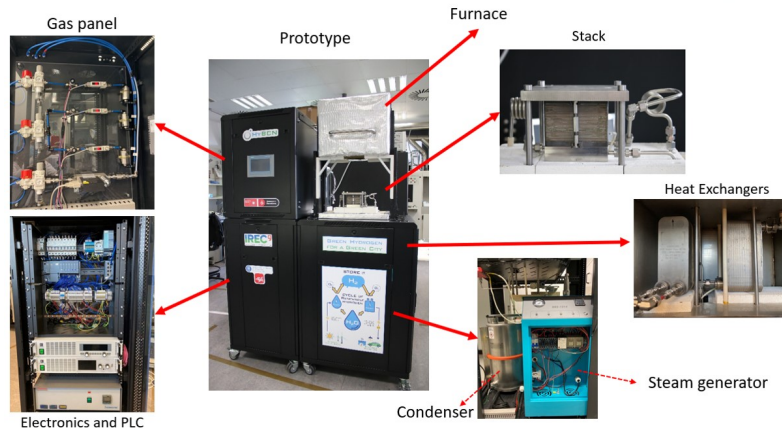
Figure 1: Description of the main elements in the IREC Reversible Solid Oxide Testing Prototype [21]

mixture of H_2O with a small amount of H_2 (around 10%) to maintain the fuel electrode reduced and air at the oxygen side [22, 23].

2.2. Flow Impact in SOFC-SOEC Power Response

The first experimental tests evaluate the impact of the gas flow on the stack power performance, when the stack remain in one operating mode (SOEC or SOFC) during the entire experiment. This allows us to obtain a baseline behavior to compare with the response during mode transitions.

Performance characterization for different gas flow conditions was done by performing polarization curves, which consists in gradually increase the current while recording the voltage evolution. A sweeping rate of 40 A/min was used. Flow were changed on both electrodes at the time, always keeping a volumetric ratio of 2.5 between H_2 and air, in order to respect the stoichiometry of the reactions (water electrolysis or hydrogen reduction). The change in flow was performed, gradually increasing the hydrogen and air flows until reaching the desired values, to subsequently increase the current with steps of one ampere. The polarization curves in SOFC mode, presented in Figure 2 correspond to flows of 5 NL/min of H_2 and 12.5 NL/min of air, 10 NL/min of H_2 and 25 NL/min of air and 15 NL/min H_2 and 37.5 NL/min of air. On the other hand, in SOEC mode, the polarization curves from Figure 3 correspond to flows of 5 NL/min, 10 NL/min, 15 NL/min of H_2O. For all cases, the air flow was set to 26 NL/min.

Figure 2 shows the effect of different H_2 flows on the voltage and power responses. It is possible to observe that the lower flows of H_2, (5 NL/min), means achieving low power levels reaching 65.8% percent of fuel utilization. The increase in the flows implies a greater amount of delivered power with flows of 10 NL/min or 15 NL/min, but decreasing the fuel utilization to 40% or less. This change is mainly related to two phenomena. One is the decrease of the Nernst potential by the gas flow increase. It corresponds to 20% of the voltage difference at 0.2 A/cm^2 (around 0.7 V when increasing the fuel flow from 5 NL/min to 15 NL/min and 2.5 times the air flow in comparison with measured values

3.44 V). The second is the reduction of the concentration overpotential, having higher flow helps bringing new reactants close to the reactive point and evacuating the products.

The voltage and power responses in SOEC mode can be seen in Figure 3. Similarly, higher flow of H_2O allows reaching power levels close to the rated values of the stack (with 15 NL/min of H_2O), with low fuel utilization. These results suggest that the operation at rated powers of the reversible solid oxide system is reached with the highest flow in both modes. In the analyzed case, 90% of H_2O–10% of H_2 and 100% H_2 with a flow of 15 NL/min seem to be the most appropriate flows for the best exploitation of the rSOC in both operation modes. These experiments were carried out at 750°C.
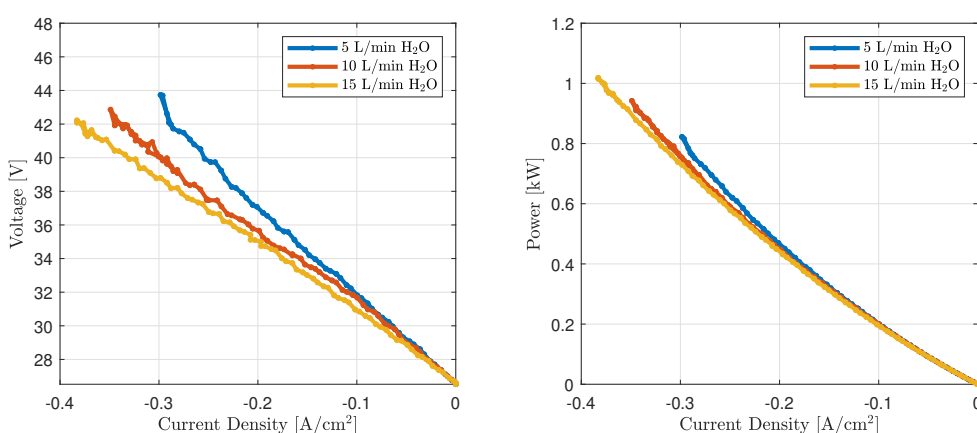
2.3. Transition Cycles

This section analyzes the response times of the transition between the different operating conditions. These experiments consist in reaching the rated power at constant composition and flow in one mode (SOFC or SOEC), and switching from one mode to the other (SOFC to SOEC or SOEC to SOFC). In this last configuration, two scenarios are studied: without changing the gas conditions and adapting the gas conditions to the optimal ones before switching between the two modes.

More precisely, the experiments were carried out imposing a maximum injection limited to 40 A/min followed by a series of safety protocols, in order to avoid rapid degradation of the electrolyte causing a decrease in the stack performance. Mainly, two safety protocols were imposed to ensure the safe operation of the system. The first protocol aims to restrict stack temperature variations to a maximum of 30°C compared to the current value. The second protocol involves limiting the voltage values to 0.6 V per cell in SOFC mode (equivalent to 18 V for the full stack of 30 cells) and to 1.4 V per cell in SOEC mode (equivalent to 42 V for the full stack). Once the safety voltage threshold is reached, the current profile is automatically reset to 0 A, ensuring optimal safety conditions.
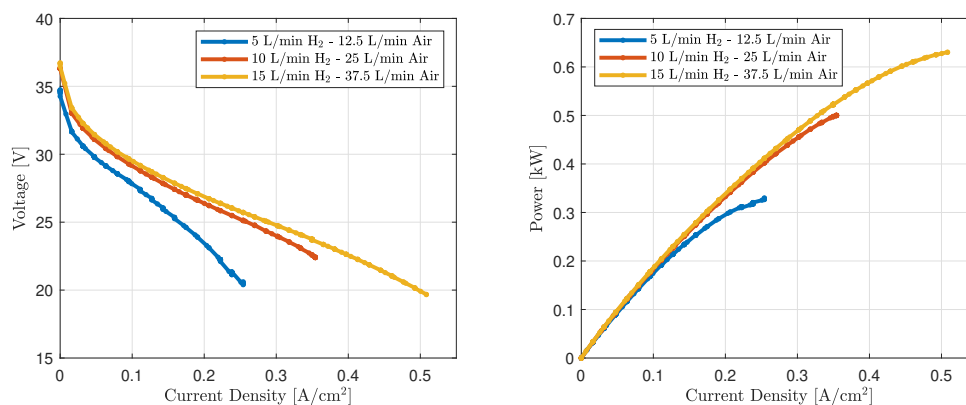
Figure 2: Effect of the gas flow on the polarization curves and power response in SOFC mode

Figure 3: Effect of the gas flow on the polarization curves and power response in SOEC mode

Firstly, the transition cycles are analyzed keeping the inlet flows constant on both electrodes. Therefore, to be able to work in SOFC and SOEC mode, the fuel composition is fixed to 50% of H_2 and 50% of H_2O at 750°C. The experimental results are presented in Figure 4. The transition cycle corresponds to SOFC→SOEC→SOFC. It is possible to observe that the system is able to reach the rated power value only in SOEC mode and close to half the rated value in SOFC. Indeed, this non-symmetric behaviour can partially be explained by the difference of gas diffusion when the atmosphere is richer in H_2 or in H_2O [24]. At high current densities, around 0.3 A/cm^2 for this stack, concentration over-potential at the fuel electrode becomes dominant. In SOEC mode, the produced H_2 is added to the initial H_2, which is a small molecule in comparison with H_2O. Its diffusion through the porosity of the fuel electrode is therefore easier than in the case of SOFC where there is an accumulation of H_2O when consuming the H_2.

Figures 5 and 6 shows the experimental responses under changes in the power set-points when rSOC remains in one operating mode. Figure 5 corresponds to a change in the power set-point from 0 kW to 1 kW and back to 0 kW with the rSOC operating in SOEC mode. Figure 6 presents the
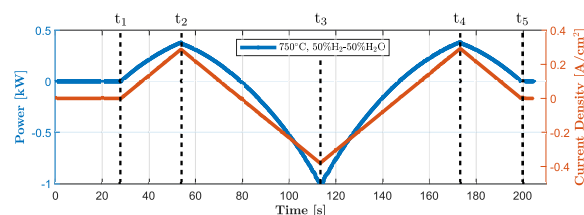

	t_1	t_2	t_3	t_4	t_5
Time [s]	28.0	53.6	113.4	173.2	199.0
Power [kW]	0.00	0.379	-1.00	0.38	0.00

Figure 4: Experimental power results corresponding to SOFC-SOEC-SOFC direct transitions at 750°C with 50%H_2 and 50%H_2O (10,4 NL/min) and 26 NL/min of air.

results corresponding to a similar scenario but when the rSOC remains in SOFC mode and the maximum power set-point is 0.3 kW. It is possible to observe that the duration of transitions are lower than a minute in each mode of operation.
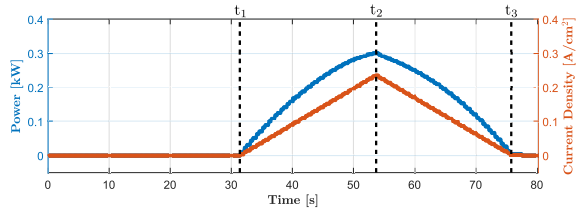
The final test analyzes a transition cycle from SOEC to SOFC with a change in fuel composition. The most
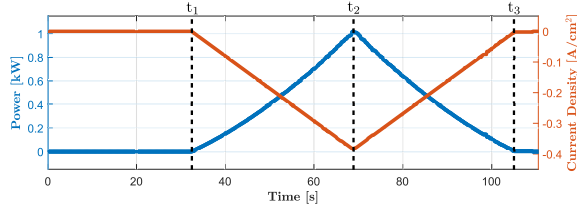
	t_1	t_2	t_3
Time [s]	32.4	68.8	105.2
Power [kW]	0.00	1.02	0.00

Figure 5: Experimental response corresponding to a change in the power set-point from 0 kW to 1 kW and back to 0 kW in SOEC mode, with 10 NL/min of H_2O, 1.1 NL/min of H_2 and 26 NL/min of air
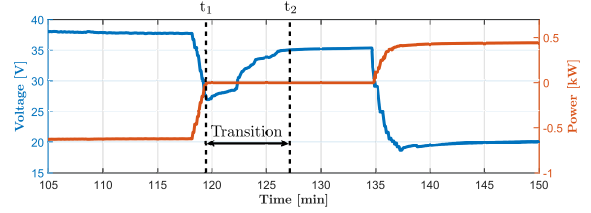

	t_1	t_2	t_3
Time [s]	31.4	53.8	76.6
Power [kW]	0.00	0.304	0.00

Figure 6: Experimental response corresponding to a change in the power set-point from 0 kW to 0.3 kW and back to 0 kW in SOFC mode, with 10 NL/min of H_2 and 26 NL/min of air.

demanding case consists in a transition from a rich H_2O concentration (i.e. 90% H_2O and 10% H_2O) in SOEC mode to a rich hydrogen concentration (100% H_2) in SOFC mode. The result of this test is presented in Figure 7. Initially, the cell operates in SOEC mode with a concentration of 90% H_2O 10% H_2. At $t_1 = 119.5$ minutes, the power becomes zero (zero current) and the concentration changes until reaching 100% H_2. In Figure 7, the change in open circuit voltage or Nernst potential until the partial pressure of H_2 and H_2O are being stables can be appreciated, specifically between the instants t_1 and t_2, a period of about 8 minutes. As the voltage must remain constants for a suitable stack performance, this indicates that it is necessary to wait approximately 8 minutes to switch from one mode to the other. This transition time is important when the rSOC operates within a microgrid since this imposes a time interval in which the stack cannot supply power and must be compensated by other generators.

3. Transition Impacts on Microgrid Operation

In this section, the impact of the response times of the rSOC on a microgrid is analyzed by simulations. For this purpose, the rSOC is integrated into a microgrid including other renewable energy sources under different operating scenarios.

	t_1	t_2
Time [min]	119.5	127.7
Stack Voltage [V]	26.94	35.10

Figure 7: Experimental results corresponding to a transition cycle from SOEC to SOFC with concentration change from 90%H_2O-10%H_2 (SOEC) to 100% H_2 (SOFC)

3.1. Model for Microgrid Analysis

In order to include the experimental dynamics shown in the previous section in a desired microgrid, the dynamic model developed in our previous work [21] is used. The basis of dynamic model relies on electrochemistry and thermodynamics principles, which able us to obtain the voltage and power values of the rSOC each time instant, being the commands entering to the microgrid. The electrochemical behavior determine the operating voltage of the cell (V_c) in each mode. In SOFC mode, V_c is given by:

$$V_{SOFC} = E_N - \eta_{ohm} - \eta_{act} - \eta_{con}, \quad (1)$$

and in SOEC mode, as the injected current is negative, by:

$$V_{SOEC} = E_N + \eta_{ohm} + \eta_{act} + \eta_{con}, \quad (2)$$

being E_N the Nernst voltage, η_{ohm} ohmic losses, η_{act} the activation losses and η_{con} the concentration losses. The ohmic losses are dominated by the current density $\mathcal{I}$ (in A/cm^2) and the specific area resistance (ASR) per cm^2 as

$$\eta_{ohm} = \mathcal{I} \cdot ASR. \quad (3)$$

Activation losses are related to the kinetics of the chemical reactions that take part in the process, and are defined by:

$$\eta_{act} = \frac{RT}{4\alpha_a F}\sinh^{-1}\left(\frac{i}{2i_{o,a}}\right) + \frac{RT}{4\alpha_c F}\sinh^{-1}\left(\frac{i}{2i_{o,c}}\right). \quad (4)$$

Finally, concentration losses are dominated by changes in the concentration of the reactants at the Triple-Phase Boundary (TPB), as:

$$\eta_{con} = \underbrace{\frac{RT}{2F}\ln\left(\frac{p_{H_2O}^{TPB}p_{H_2}}{p_{H_2O}p_{H_2}^{TPB}}\right)}_{\text{Anode}} + \underbrace{\frac{RT}{4F}\ln\left(\frac{p_{O_2}}{p_{O_2}^{TPB}}\right)}_{\text{Cathode}}. \quad (5)$$

Finally, to ensure a safe thermodynamic behavior of the system, the thermal balance of the rSOC system is defined by:

$$\Delta\dot{Q} = \dot{Q}_{stack} + \dot{Q}_{ov} - \dot{Q}_{con} - \dot{Q}_{env}, \quad (6)$$
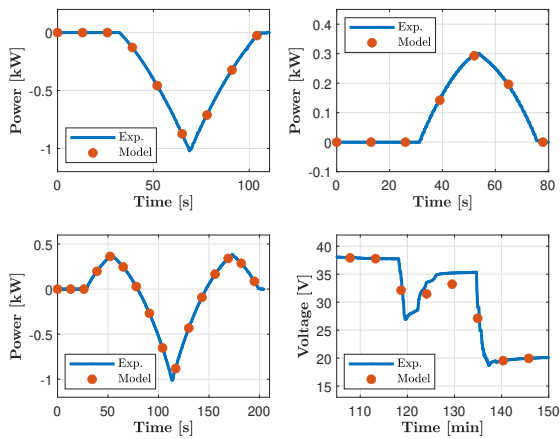
Figure 8: Comparison between experimental transitions (Figures 4 to 7) and model response: a) SOEC Mode, b) SOFC Mode, c) SOFC-SOEC-SOFC 50%-50% and d) Transition with change of composition

where $\dot{Q}_{stack}$ is the stack heat, $\dot{Q}_{ov}$ the oven heat losses, $\dot{Q}_{con}$ the convection losses and $\dot{Q}_{env}$ the environmental losses. Once the voltage is obtained, the power of the cells can be calculated according to the ohms law as:

$$P = n_c \mathcal{I} V_c. \tag{7}$$

The description of the mentioned variables and their values can be found in Table 2. Figure 8 presents a comparison of responses in relation to the experiments presented in Figures 4 to 7. The model dynamics are similar to the experimental response of the system, as presented in the previous validation of the model [21] and respect the transition times of the experiments, which is important for a reliable integration in the microgrid. A thorough validation and more details of the rSOC operation can be found in our previous work [21].

3.2. Microgrid Analysis: An Islanded Approach
In order to evaluate the rSOC capabilities within a electrical network, the microgrid illustrated in Figure 9 is used. This microgrid consists of three inverters: two interfacing generators and another connecting the rSOC. The generators in Figure 9 correspond to renewable power sources (wind, solar, etc.) and also to energy storage devices (BESS, compressed air storage, etc.), being able to replicate for example house-level applications (e.g. PV+Storage), higher power applications (e.g. Wind+Storage) or industrial grids (e.g. Diesel or Gas Generators). The rSOC dynamics are introduced as modeled in Section 3.1. The green areas indicate the units of the microgrid delivering power whereas the red ones denote the units absorbing power. The components of the microgrid have been sized according to the reversible solid oxide prototype characteristics. The grid-forming operation of the microgrid is controlled through the droop control, a strategy widely known in the literature [25]. The

Table 2
Reversible Solid Oxide Stack Parameters [21]

Stack Parameter	Symbol	Value	Units
Stack Area	A_s	63	cm^2
Stack Mass	M_s	5.5	kg
Faraday Constant	F	96485	C/mol
Number of Cells	n_c	30	-
Oven Power	P_{ov}	2.75	kW
Oven Losses Constant	$k_{l,ov}$	0.7	$W/(m^2 \cdot K)$
Universal Gas Constant	R	8.314472	$J/(mol \cdot K)$
Air Gas Constant	R_{air}	286.9	$J/(kg \cdot K)$
Inlet Manifold Valve Constant	$\mathcal{K}_{im}$	$5 \cdot 10^{-8}$	$kg/(Pa \cdot s)$
Outlet Manifold Valve Constant	$\mathcal{K}_{om}$	$3.3 \cdot 10^{-8}$	$kg/(Pa \cdot s)$
Anode Valve Constant	$\mathcal{K}_{an}$	$1.5 \cdot 10^{-8}$	$kg/(Pa \cdot s)$
Cathode Valve Constant	$\mathcal{K}_{ca}$	$0.94 \cdot 10^{-8}$	$kg/(Pa \cdot s)$
Electrolyte Thickness (8YSZ)	L_e	10	μm
O_2 Effective Diffusion Coefficient	D_{O_2}	0.0228	cm^2/s
H_2O Effective Diffusion Coefficient	D_{H_2O}	0.0436	cm^2/s
H_2 Effective Diffusion Coefficient	D_{H_2}	0.0927	cm^2/s
Hydrogen Lowest Heating Value	H_2^{LHV}	241.8	kJ/mol
Ionic Conductivity Pre-exponential Factor	$\sigma_{0,el}$	466	s^{-1}
Electrolyte Activation Energy	E_{el}	$8.26 \cdot 10^4$	J/mol
Cathode Phenomenological Coefficient	γ_{ca}	$5.23 \cdot 10^6$	A/cm^2
Anode Phenomenological Coefficient	γ_{an}	$6.64 \cdot 10^6$	A/cm^2
Cathode Activation Energy	$E_{act,ca}$	10^5	J/mol
Anode Activation Energy	$E_{act,an}$	$7.96 \cdot 10^4$	J/mol
Contact Resistance	R_{ct}	0.3	Ω
Degradation Rate [7]	κ	1.2	$m\Omega cm^2/kh$
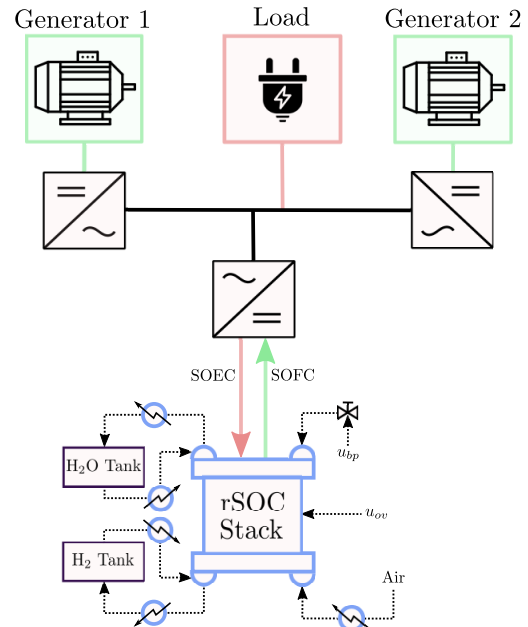
Figure 9: Islanded microgrid with two generators, a rSOC and a load. Green areas denote the units delivering power whereas the red ones denote the units absorbing power.

fundamental aspects of this type of control are introduced next.

The primary control is implemented with a droop scheme that adjusts the power supplied by each converter by regulating the frequency and voltage amplitude. The droop control

allows the system inverters to work in parallel sharing the network load by changing the angular frequency ω_k of the inverter according to:

$$\omega_k = \omega - m_k P_k, \tag{8}$$

where ω_n is the nominal grid frequency and m_k the droop coefficient with respect to the active power P_k. On the other hand, the voltage control law is as follows:

$$V_k = V - n_k Q_k, \tag{9}$$

where V_k is the output voltage of the inverter, V is the nominal voltage of the network and n_k is the droop coefficient with respect to the reactive power Q_k. Finally, the secondary control adds two terms to the droop expressions (8) and (9) resulting:

$$\omega_k = \omega - m_k P_k + \delta_k^\omega \tag{10}$$

$$V_k = V - n_k Q_k + \delta_k^V, \tag{11}$$

where δ_k^ω and δ_k^V are the frequency and voltage corrections computed according to the averaging technique as:

$$\delta_k^\omega = k_p^\omega \left(\omega^* - \overline{\omega} \right) + k_i^\omega \int \left(\omega^* - \overline{\omega} \right) dt \tag{12}$$

and

$$\delta_k^{\overline{V}} = k_p^\omega \left(V^* - \overline{V} \right) + k_i^V \int \left(V^* - \overline{V} \right) dt$$
$$\delta_i^{\overline{Q}} = k_p^Q \left(\overline{Q} - Q_k \right) + k_i^Q \int \left(\overline{Q} - Q_k \right) dt \tag{13}$$

where $\delta_i^V = \delta_i^{\overline{V}} + \delta_i^{\overline{Q}}$, $\overline{V}$ and $\overline{Q}$ denotes the average voltage amplitude and reactive power, respectively, and k_p^ω, k_i^ω, k_p^V, k_i^V, k_p^Q and k_i^Q are proportional and integral control parameters.

More details about the design of this microgrid control scheme can be find in e.g. [1, 2, 25]

3.3. Modes of Operation

The capability of rSOC to operate in islanded microgrid is analyzed here with two scenarios, which include the operation of the rSOC inverter in grid-following and grid-forming. The results indicate that the grid-following operation seems to be the most suitable scheme for the rSOC.

3.3.1. Grid-following Mode

In the grid-following operation, the rSOC absorbs and supplies power to the microgrid. Due to grid-following is the most probable mode of operation, the response of the microgrid considering direct mode change, with a 50%-50% composition (H_2-H_2O), and considering the transition cycle, will be analyzed.

- **Transition cycle with a 50%H_2-50%H_2O composition**: The results of a direct change mode are presented in Figure 10. It can be seen that the increase in the
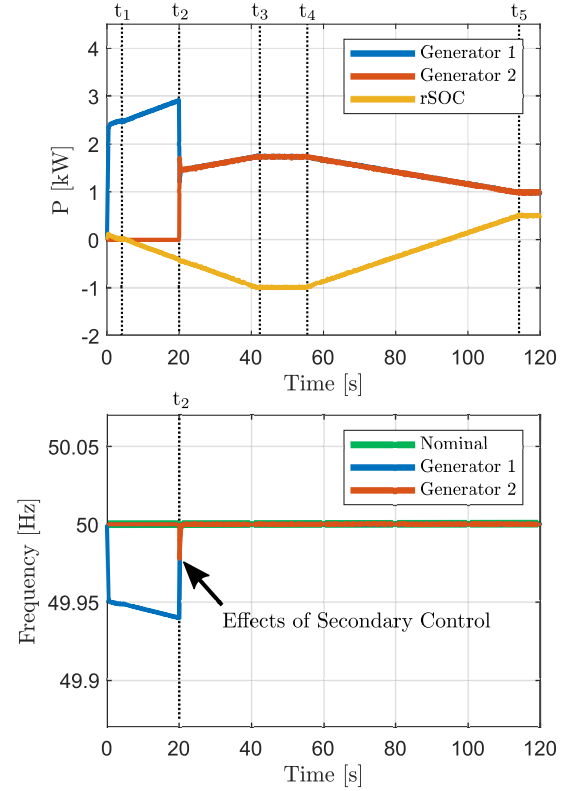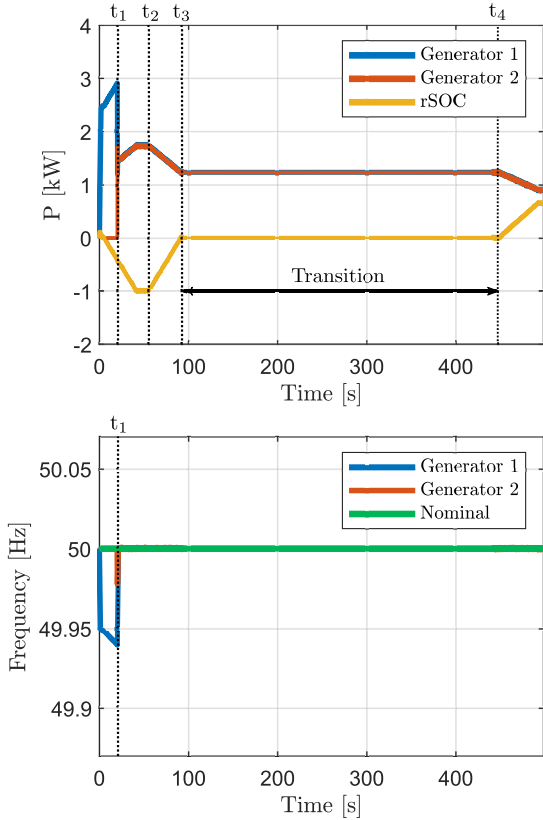

Figure 10: Active power and frequency responses of the microgrid with the rSOC acting in grid-following mode and with a direct-mode change with 50%-50% H_2-H_2O at 750°C.

power of generator 1 to satisfy the load and the energy necessary to carry out the electrolysis at $t_1 = 5$ s. At $t_2 = 19.5$ s, when the generator 1 reaches its power limits (3 kW), the generator 2 must be activated in order to supply the additional power demanded by the load and the rSOC. It can be observed the proper operation of the power sharing algorithm and the secondary control as they are able to balance the power and restore the frequency to their nominal values. At $t_3 = 41.4$ s the SOEC mode reach 1 kW, and performs the electrolysis up to $t_4 = 55$s, when the direct transition of SOEC mode to SOFC mode starts. When this direct transition from electrolyzer mode to fuel cell mode occurs, it can be seen how the power of generators 1 and 2 is reduced, according to the amount of power injected by the rSOC. At $t_5 = 114.6$s, the power delivered by the rSOC reaches a value around 0.4 kW in SOFC mode. Notice that during the entire transition cycle, the secondary control maintains the frequency close to 50 Hz with the contributions of generators 1 and 2, demonstrating its robustness under power changes. As expected, the slow dynamics of the rSOC governs the entire system response.

- **Transition cycle with change of composition:** Figure 11 shows the active powers of rSOC and the generators and the frequencies of inverters 1 and 2 during a transition cycle from 90% H_2O and 10% H_2 in SOEC
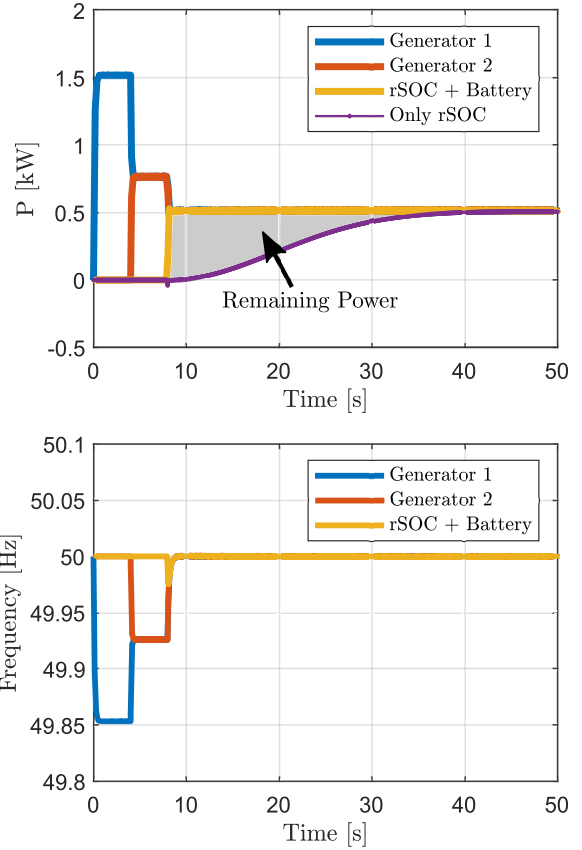
Figure 11: Active power and frequency responses of the microgrid with the rSOC acting in grid-following mode and with a transition cycle from 90%-10% H_2-H_2O to 100% H_2 at 750°C.

Figure 12: Active power and frequency responses of the system in grid-forming operation. In grey, the necessary power from a battery for operating in grid-forming.

mode to 100% H_2 in SOFC mode. As shown in Figure 7, the transition cycle increases the operation times since the rSOC needs at least 8 minutes to completely change the operating mode. Nevertheless, it can be seen that the power and frequency responses are similar to the previous case. The droop and secondary controls are able to maintain the frequency close to the nominal value by properly commanding the two generators to compensate the power supplied or absorbed by the rSOC. Therefore, in terms of dynamic performance, the transition cycle does not alter the microgrid behavior, increases the rSOC performance compared to the direct mode change due to higher power in each mode when higher fuel concentration is achieved and thus improves the efficiency of the overall system.

3.3.2. Grid-Forming mode: What is needed?

The second scenario presents the behavior of the system with the rSOC inverter working in grid-forming. This mode of operation can only be carried out in SOFC mode. This operating mode can be useful in case the other generators are not able to provide their maximum power and the levels of H_2 stored are high. In this way, the rSOC inverter is able to contribute in the power sharing algorithm. However, this need the help of a fast-response energy storage system, as

for example, lithium batteries, due to the response times of the rSOC technology. Also, note that for operating in the power sharing algorithm, rSOCs must maintain certain thermal effects to ensure a safe constant power delivery.

Figure 12 compares the behavior of the microgrid operating in grid-forming mode with and without a battery energy storage to provide the necessary fast power compensation. The purple line corresponds to the power delivered by the rSOC working alone and the yellow line to the power contributed when the rSOC operates along with a battery. Clearly, it can be seen that in the first case the power sharing algorithm is not able to ensure the necessary fast response contrary to the second case. The grey area indicates the total amount of power that must be supplied by the battery for the correct operation of the islanded microgrid, in which the dynamics is not directly dominated by the hydrogen power response. Without this amount of power the microgrid operation will become unstable. Therefore, only a proper operation could be achieved with the use of a battery and a rSOC, as shown in the frequency response plot.

4. Conclusions

Reversible solid oxide cells have the potential for being a key technology in the transition to hydrogen-based societies, thanks to the higher efficiency and fuel flexibility. This work

has studied one of the most challenging factors for their use in electrical systems: the rSOC power response times. Dynamics of rSOC operation were experimentally obtained by testing a 0.7-1kW SOFC-SOEC stack. Transition cycles for reaching rated power levels in SOEC, SOFC and from one mode to the other were performed. The results allow us to determine the order of magnitude of the different transitions: from zero to rated power is less than 1 minute, and less than 8 minutes for the transition cycles SOEC-SOFC, suggesting that the total transition time from rated SOEC power to rated SOFC power should take at least 10 minutes. The transition time dynamics in a certain microgrid, introduced by using the experimental validated rSOC model, have shown a significant impact on electrical grid operations. This is especially relevant in islanded microgrids, since the other generators in the microgrid must compensate the load demand and ensure the frequency stability. As the slow dynamics of the rSOC tends to dominate the overall microgrid dynamics, the rSOC should operate in grid-following mode absorbing or generating power in SOEC or SOFC modes, respectively. For a proper operation in grid-forming mode, the rSOC must be complemented with a fast power source as batteries in order to avoid microgrid instabilities.

Acknowledgements

CRediT authorship contribution statement

Hector del Pozo Gonzalez: Conceptualization, Methodology, Software, Data curation, Visualization, Investigation, Writing - Original draft preparation. **Lucile Bernadet:** Conceptualization, Investigation, Data curation, Validation, Writing - Original draft preparation. **Marc Torrell:** Conceptualization, Investigation, Funding, Validation. **Fernando D. Bianchi:** Conceptualization, Investigation, Validation, Visualization, Writing - Original draft preparation. **Albert Tarancón:** Supervision, Funding, Validation. **Oriol Gomis-Bellmunt:** Supervision, Validation, Writing- Reviewing and Editing. **Jose Luis Dominguez-Garcia:** Supervision, Funding, Validation, Writing - Reviewing and Editing.

References

[1] Antonio Carlos Zambroni de Souza and Miguel Castilla. *Microgrids design and implementation*. Springer, 2019.

[2] Daniel E Olivares, Ali Mehrizi-Sani, Amir H Etemadi, Claudio A Cañizares, Reza Iravani, Mehrdad Kazerani, Amir H Hajimiragha, Oriol Gomis-Bellmunt, Maryam Saeedifard, Rodrigo Palma-Behnke, et al. Trends in microgrid control. *IEEE Transactions on Smart Grid*, 5(4):1905–1919, 2014.

[3] Timothy D Hutty, Siyuan Dong, and Solomon Brown. Suitability of energy storage with reversible solid oxide cells for microgrid applications. *Energy Conversion and Management*, 226:113499, 2020.

[4] Alexander Buttler and Hartmut Spliethoff. Current status of water electrolysis for energy storage, grid balancing and sector coupling via power-to-gas and power-to-liquids: A review. *Renewable and Sustainable Energy Reviews*, 82:2440–2454, 2018.

[5] Kewei Hu, Jiakun Fang, Xiaomeng Ai, Danji Huang, Zhiyao Zhong, Xiaobo Yang, and Lei Wang. Comparative study of alkaline water electrolysis, proton exchange membrane water electrolysis and solid oxide electrolysis through multiphysics modeling. *Applied Energy*, 312:118788, 2022.

[6] Suhas Nuggehalli Sampathkumar, Philippe Aubin, Karine Couturier, Xiufu Sun, Bhaskar Reddy Sudireddy, Stefan Diethelm, Mar Pérez-Fortes, et al. Degradation study of a reversible solid oxide cell (rsoc) short stack using distribution of relaxation times (drt) analysis. *International Journal of Hydrogen Energy*, 47(18):10175–10193, 2022.

[7] Elisa Zanchi, Antonio Gianfranco Sabato, Mari Carmen Monterde, Lucile Bernadet, Marc Torrell, José Antonio Calero, Albert Tarancón, and Federico Smeacetto. Electrophoretic deposition of MnCo2O4 coating on solid oxide cell interconnects manufactured through powder metallurgy. *Materials & Design*, 227:111768, 2023. ISSN 0264-1275.

[8] M Reytier, S Di Iorio, A Chatroux, M Petitjean, J Cren, M De Saint Jean, J Aicart, and J Mougin. Stack performances in high temperature steam electrolysis and co-electrolysis. *International Journal of Hydrogen Energy*, 40(35):11370–11377, 2015.

[9] L. Bernadet, G. Gousseau, A. Chatroux, J. Laurencin, F. Mauvy, and M. Reytier. Influence of pressure on solid oxide electrolysis cells investigated by experimental and modeling approach. *International Journal of Hydrogen Energy*, 40(38):12918–12928, 2015. ISSN 0360-3199.

[10] Jérôme Aicart, Stéphane Di Iorio, Marie Petitjean, Pascal Giroud, Géraldine Palcoux, and Julie Mougin. Transition cycles during operation of a reversible solid oxide electrolyzer/fuel cell (rsoc) system. *Fuel Cells*, 19(4):381–388, 2019.

[11] S Srikanth, MP Heddrich, S Gupta, and KA Friedrich. Transient reversible solid oxide cell reactor operation–experimentally validated modeling and analysis. *Applied Energy*, 232:473–488, 2018.

[12] Ro Peters, M Frank, W Tiedemann, Ingo Hoven, Robert Deja, N Kruse, Q Fang, L Blum, and Ra Peters. Long-term experience with a 5/15kw-class reversible solid oxide cell system. *Journal of the Electrochemical Society*, 168(1):014508, 2021.

[13] Felix Garcia-Torres, Luis Valverde, and Carlos Bordons. Optimal load sharing of hydrogen-based microgrids with hybrid storage using model-predictive control. *IEEE Transactions on Industrial Electronics*, 63(8):4919–4928, 2016.

[14] Xiangjun Quan, Qinran Hu, Xiaobo Dou, Zaijun Wu, Ling Zhu, and Wei Li. Control of grid-forming application for fuel cell/electrolyser system. *IET Renewable Power Generation*, 14(17):3368–3374, 2020.

[15] YH Li, Sumedha Rajakaruna, and SS Choi. Control of a solid oxide fuel cell power plant in a grid-connected system. *IEEE Transactions on Energy Conversion*, 22(2):405–413, 2007.

[16] M Califano, M Sorrentino, MA Rosen, and C Pianese. Optimal heat and power management of a reversible solid oxide cell based microgrid for effective technoeconomic hydrogen consumption and storage. *Applied Energy*, 319:119268, 2022.

[17] F Vitale, N Rispoli, M Sorrentino, MA Rosen, and C Pianese. On the use of dynamic programming for optimal energy management of grid-connected reversible solid oxide cell-based renewable microgrids. *Energy*, 225:120304, 2021.

[18] N Rispoli, F Vitale, F Califano, M Califano, P Polverino, MA Rosen, and M Sorrentino. Constrained optimal design of a reversible solid oxide cell-based multiple load renewable microgrid. *Journal of Energy Storage*, 31:101570, 2020.

[19] Konrad Motylinski, Jakub Kupecki, Bart Numan, Yashar S Haji-molana, and Vikrant Venkataraman. Dynamic modelling of reversible

solid oxide cells for grid stabilization applications. *Energy Conversion and Management*, 228:113674, 2021.

[20] Arianna Baldinelli, Linda Barelli, and Gianni Bidini. Progress in renewable power exploitation: Reversible solid oxide cells-flywheel hybrid storage systems to enhance flexibility in micro-grids management. *Journal of Energy Storage*, 23:202–219, 2019.

[21] Hector del Pozo Gonzalez, Marc Torrell, Lucile Bernadet, Fernando D Bianchi, Lluís Trilla, Albert Tarancón, and Jose Luis Domínguez-García. Mathematical modeling and thermal control of a 1.5 kw reversible solid oxide stack for 24/7 hydrogen plants. *Mathematics*, 11(2):366, 2023.

[22] Christopher Graves, Sune Dalgaard Ebbesen, Søren Højgaard Jensen, Søren Bredmose Simonsen, and Mogens Bjerg Mogensen. Eliminating degradation in solid oxide electrochemical cells by reversible operation. *Nature materials*, 14(2):239–244, 2015.

[23] S Diethelm, J Van herle, D Montinaro, and O Bucheli. Electrolysis and co-electrolysis performance of soe short stacks. *Fuel Cells*, 13 (4):631–637, 2013.

[24] E Da Rosa Silva, Giuseppe Sassone, Manon Prioux, Maxime Hubert, Bertrand Morel, and Jerome Laurencin. A multiscale model validated on local current measurements for understanding the solid oxide cells performances. *Journal of Power Sources*, 556:232499, 2023.

[25] Joan Rocabert, Alvaro Luna, Frede Blaabjerg, and Pedro Rodriguez. Control of power converters in ac microgrids. *IEEE Transactions on Power Electronics*, 27(11):4734–4749, 2012.